Human and Mouse Models for Kabuki Syndrome Reveal Increase in Inhibitory Synapse Development.

Short title: Altered synapse development in Kabuki syndrome

James Knopp[1], Alexander Weaver[1], Sean Miller[1], Toshihiro Nomura[2], Ava Whitlark[1], Jack Swantkowski[1], Alexandra Noble[1], Sandy Nam[1], Katharyn Hutson[1], Jenny Bergqvist-Patzke[1], Anis Contractor[2] and Christopher Patzke[1*].

[1] Department of Biological Sciences, Boler-Parseghian Center for Rare Diseases, University of Notre Dame, Notre Dame, IN, USA

[2] Department of Neuroscience, Feinberg School of Medicine, Northwestern University, Chicago, Illinois, USA

*Address correspondence to: Christopher Patzke, 109A Galvin Life Science Center, University of Notre Dame, Notre Dame, IN 46556
Email: cpatzke@nd.edu

ABSTRACT

Intellectual disability, affecting 2-3% of the general population, often coincides with neurodevelopmental disorders and is frequently caused by mutations that impair synaptic function. Kabuki syndrome (KS), a rare multisystem disorder associated with developmental delay and intellectual disability, results from mutations in either *KMT2D* (KS type 1) or *KDM6A* (KS type 2), which encode a chromatin-modifying methyltransferase and demethylase, respectively. However, the mechanisms contributing to intellectual disability in KS remain poorly understood. Here, we generated human iPS cells carrying a conditional Cre/lox-dependent *KMT2D* or *KDM6A* loss-of-function mutation, used for directed differentiation into inhibitory or excitatory neurons. Analysis of Cre-mediated induction of KS type 1 and KS type 2 in inhibitory neurons unexpectedly revealed an increase in GABAergic synapse development. Mutant excitatory neurons, however, displayed a reduction in synapse development and impaired information transfer within neural networks. We confirmed these findings in hippocampal neurons *in vitro* and *in vivo* using a mouse model for KS type 1. Synapse numbers and synaptic transmission in acute brain slices were shifted to increased inhibition/excitation ratio. Thus, our results, using purely inhibitory or purely excitatory human neurons with conditional deletion of *KMT2D* or *KDM6A,* and mouse with *Kmt2d* deletion, reveal a novel disease mechanism of KS and provide a mechanistic explanation for intellectual disability observed in individuals affected by KS highlighting imbalanced excitation to inhibition in neural circuits.

INTRODUCTION

Kabuki syndrome (KS) is a rare multisystem autosomal dominant disorder associated with developmental delay and intellectual disability, affecting approximately 1 in 32,000 births. It is caused by heterozygous/hemizygous loss-of-function mutations in either the *KMT2D* gene (KS type 1: 70% of cases) or the *KDM6A* gene (KS type 2: up to 5% of cases) (Boniel et al., 2021). *KMT2D* (also called *MLL2* or *MLL4*) on chromosome 12q13 encodes a histone 3 lysine 4 mono-, di-, and tri-methylase (H3K4me1-3), while the X-linked *KDM6A* (also called *UTX*) is a histone 3 lysine 27 trimethyl (H3K27me3) demethylase (Agger et al., 2007; Dhar et al., 2012; Hong et al., 2007; Lan et al., 2007; Lee et al., 2013; Li et al., 2011; Miyake et al., 2013; Ng et al., 2010). *KDM6A* has been reported to escape X inactivation and has a homologue on the Y chromosome: *UTY* (Greenfield et al., 1998; Walport et al., 2014). KMT2D and KDM6A are tumor suppressors and mutations are found in many types of cancer (Egolf et al., 2021; Lawrence et al., 2014; Van et al., 2024; Wu et al., 2018; Zhang et al., 2015). KMT2D and KDM6A interact with each other in nucleus to regulate gene expression. They are found in the same multiprotein complex, the activating signal cointegrator-2-containing complex (ASCOM), and are associated with open chromatin states at promotors or enhancers, thereby epigenetically regulating chromosomal gene expression patterns during development (Barry et al., 2022; Gao et al., 2024; Lee et al., 2013). Specifically, it has been shown that

KMT2D associates with chromatin remodelers on enhancers (Park et al., 2021). Interestingly, KMT2D is required for KDM6A stability highlighted by reduced KDM6A levels in *KMT2D*- deficient cells, possibly explaining the broad overlap of clinical presentations (Lee et al., 2013).

KS type 1 and type 2 both are characterized by similar core clinical features such as distinctive facial features including long palpebral fissures and eversion of the lower eyelid (resembling the make-up of actors of Kabuki, a Japanese traditional theatrical form), postnatal growth deficiency, skeletal abnormalities, congenital malformations (e.g., cardiac defects, renal anomalies), immunological abnormalities, and up to 90% of affected individuals exhibit varying degrees of intellectual disability (Bögershausen and Wollnik, 2013; Hannibal et al., 2011; Niikawa et al., 1988; Paulussen et al., 2011). While reported animal studies elegantly revealed impaired neurogenesis in the hippocampus, associated memory defects (Benjamin et al., 2017; Bjornsson et al., 2014; Carosso et al., 2019), and improper cell differentiation (Schwenty-Lara et al., 2020; Van Laarhoven et al., 2015), the mechanisms behind patients' intellectual disability remain largely unknown. Intellectual disability is often caused by mutations that developmentally impair synapses, neural cells and their circuits. Extensive work has been done to identify and understand mutations contributing to or causing intellectual disability (Srivastava and Schwartz, 2014; Sullivan and Geschwind, 2019; Zoghbi and Bear, 2012). However, the specific effects in synaptic development and function underlying KS have not been investigated.

Here, we investigate the developmental consequences of engineered KS type 1 and KS type 2 Cre/lox-dependent mutations on synapse formation and function in human neurons, and KS type 1 in a mouse model. Our findings show that the KS mutations reduce excitatory synapse function while increasing inhibitory synaptic formation and transmission thereby repressing information flow and coordinated network activity both *in vitro* and *in vivo*. This conclusion is supported by synaptic morphological and functional changes, including alterations in synapse number, electrophysiological recordings of synaptic transmission and reduced neuronal activity, as assessed by calcium imaging.

RESULTS

Human model for Kabuki syndrome type 1 shows increased synaptic inhibition and decreased excitation

In humans, the *KMT2D* gene is located on chromosome 12 and is over 19 kilobase pairs in length containing 54 exons. To model KS type 1 in human neurons, we engineered a heterozygous conditional knockout in which exon 6 of *KMT2D* was flanked with loxP sites in human induced pluripotent stem cells (iPSCs) derived from a donor without disease-causing mutations (Patzke and Südhof, 2016). Deletion of exon 6 shifts the reading frame, effectively creating a heterozygous deletion of *KMT2D* (Fig. 1A and 1B). Next, we directly differentiated these cells by forced expression of *Ngn2 (Zhang et al., 2013)*, into purely excitatory neurons, or produced purely inhibitory neurons by expression of *Ascl1* and *Dlx2* (Yang et al., 2013). The mutation was induced via co-expression of Cre-recombinase. As

a wild-type control, we used cells treated with an inactive mutant ΔCre (Fig. 1A). We analyzed synaptic morphological changes based on three different metrics: synaptic puncta density, puncta area, and puncta intensity, which reflect synapse number and clustering. Inhibitory mutant human neurons displayed an increase in vGAT puncta density when compared to ΔCre-treated neurons, while excitatory mutant neurons exhibited a drastic decrease in the density of PSD95-positive puncta (Fig. 1C-F), which shows a morphological synaptic shift to increased inhibition and reduced excitation in mutant human neurons. Interestingly, we detected an increased length and number of dendrites but no change of axonal morphology in mutant neurons (Suppl. Fig.1). To determine the functional consequences of the *KMT2D* mutation, we performed GCaMP8m-based calcium imaging experiments. First, we examined excitatory human neurons and observed a decreased event frequency per mutant neuron with higher signal amplitude but no differences in the average frequency of synchronously firing cell (per view field) (Fig. 1G-K). Second, we probed inhibitory neurons and detected an overall decrease in calcium activity in all cells and synchronously firing cells (Suppl. Fig. 2). Together, these results suggest that the heterozygous Cre/Lox-dependent deletion of *KMT2D* and the consequential morphological synaptic changes reduce neuronal activity in both excitatory and inhibitory by decreasing excitatory and increasing inhibitory synaptic communication.

Human model for Kabuki syndrome type 2 shows increased inhibitory synaptic puncta parameters and decreased excitatory communication

Next, we asked whether induction of KS type 2 in human neurons would cause the same effect as observed in the human KS type 1 model system. We flanked exon 7 of the *KDM6A* gene with loxP sites in otherwise wild-type iPSCs derived from a male donor (same donor as used for our human KS type 1 model), thereby creating a conditional hemizygous knockout (Fig. 2A). Cre-expression led to deletion of KDM6A signal in immunocytochemistry (Fig. 2B). In parallel with the induction of the KS type 2-causing mutation by treatment with Cre, we differentiated these engineered cells into inhibitory human neurons, labeled GABAergic synapses for vGAT, and detected an increase in synaptic puncta metrics (Fig. 2C-E). Next, we performed calcium imaging to assess activity in excitatory neurons. Strikingly, we observed a decrease in calcium activity in all cells and synchronously firing cells, along with an increase in signal amplitudes in *KDM6A*-mutant neurons (Fig. 2F-K). At the same time, we detected no changes in neuronal morphology (Supp. Fig. 3) Thus, the synaptic effects of *KDM6A*-mutant human neurons are similar to the phenotypes observed in *KMT2D*-mutant human neurons - increased inhibitory synaptic morphological parameters and decreased excitatory neuronal communication.

Mouse model for Kabuki syndrome type 1 shows increased number of inhibitory and decreased number of excitatory synapses in hippocampal neurons

Due to their relevance as well-established mouse disease model for KS type 1, we sought to investigate the effect of the functional heterozygous *Kmt2d* deletion on hippocampal synapses. We used heterozygous *Kmt2d*+/βGeo (Bjornsson et al., 2014) animals to analyze synaptic morphology (Fig. 3A and 3B) (Marcó de la Cruz et al., 2024; Patzke et al., 2019; Patzke et al., 2021). We labeled neurons with the presynaptic pan-neuronal markers synapsin and bassoon and found increased puncta metrics in mutant neurons (Fig. 3C-F) with increases observed particularly at distances closest to the soma (Suppl. Fig. 4A-D). To determine whether this increase was specific to excitatory or inhibitory synapses, we performed labeling and analyses of vGluT1 (excitatory presynaptic marker) and vGAT (inhibitory presynaptic marker) on the same neurons. For vGluT1, no differences were observed between wild-type (WT) and mutant (Mut) groups in terms of puncta density; however, vGluT1 area and intensity were significantly decreased, suggesting that the *Kmt2d* mutation leads to a deficit in excitatory presynaptic structures. In contrast, vGAT synaptic puncta measurements in mutant neurons showed an increase in density, area, and intensity, indicating an increase in inhibitory presynaptic structures in *Kmt2d*-mutant hippocampal neurons (Fig. 3G-J). In addition to presynaptic markers, we also assessed synaptic puncta labeled by postsynaptic markers PSD95 (excitatory), and Gephyrin (inhibitory). PSD95 puncta were markedly reduced in density and intensity, while inhibitory postsynaptic Gephyrin density was significantly increased (Fig. 3K-N). In summary, these data suggest that *Kmt2d*-mutant mouse hippocampal neurons exhibit a marked increase in inhibitory synapse metrics, accompanied by a decrease in excitatory parameters.

Mouse *Kmt2d* mutation decreases the overall number of hippocampal neurons but does not affect the number of inhibitory neurons

Because *Kmt2d*, essential for enhancer activation, is associated with defects in cell-type specific gene expression and cell differentiation, we next tested whether the number of neurons from mutant hippocampi was altered. We counted WT and Mut neurons as Map2- and DAPI-positive cells and detected a decrease in the mutant condition, consistent with previous work (Bjornsson et al., 2014). Glial cell numbers (Map2-negative cells) did not change (Fig. 4A-C). Interestingly, mutant neurons displayed longer dendrites with no alterations in the number of processes, branches, and the cell body area (Suppl. Fig. 4F-I), which was similar to our observations in the human KS type 1 model (Fig. 1). To determine whether the detected increase in inhibitory synapses in mutant neurons was due to an increased number of inhibitory neurons or the same number of inhibitory neurons forming more synapses, we examined the markers Somatostatin, Parvalbumin, and Necab1 – all of which label inhibitory neurons – and detected no changes Fig. 4D-G). Thus, these results suggest that the same number of inhibitory neurons form more synapses in *Kmt2d*-mutant neurons.

Mouse *Kmt2d* mutation leads to decreased calcium activity in hippocampal neurons.

To better understand the functional consequences of increased inhibitory synaptic development on neural networks of *Kmt2d*-mutant neurons, we performed calcium imaging (Fig. 4H and I). Our analysis revealed decreased event frequencies in individual mutant neurons, along with increased amplitudes. The synchronous (average) frequency was not changed (Fig. 4J-L). indicating that neuronal activity and communication is reduced, reflecting our findings from the human KS type 1 neurons.

Mouse *Kmt2d* mutation results in increased number of functional inhibitory synapses *in vivo*

To test whether the inhibitory phenotype observed *in vitro* is also present *in vivo*, we performed immunohistochemistry on horizontal brain sections from young adult mice (postnatal day 30) followed by confocal imaging of the hippocampal region. Consistent with our *in vitro* data, we detected a significant increase in vGAT intensity in mutant hippocampi, highlighting an increase in the number of inhibitory synapses (Fig. 5A). No difference in vGluT1 intensity was observed when compared to wild-type hippocampi (Fig. 5A-E and Suppl. Fig. 5). Thus, our data confirm that the increase of inhibitory synapses in mutant mice is relevant to hippocampal development *in vivo*. Next, we investigated the physiological consequence of increased inhibitory synapse formation in *Kmt2d*-mutant mice by recording excitatory (EPSCs) and inhibitory postsynaptic currents (IPSCs) from pyramidal neurons after stimulation of Schaffer collaterals (Fig. 5F). IPSCs and EPSCs were recorded from the same neurons. The ratio of IPSC amplitude to EPSC amplitude (I/E ratio) was measured in each cell and was compared between genotypes (WT and Mut). The I/E ratio was significantly higher in mutant mice (WT: 137.7 ± 11.6 %; Mut: 210.3 ± 21.2 %). In summary, the data from *Kmt2d*-mutant mice show that the functional development of inhibitory synapses is increased in this model for KS type 1.

DISCUSSION

In our paper we analyze newly created Cre/lox-mediated human neuron model systems for KS type 1 (Fig. 1A) and type 2 (Fig. 2A) and a mouse model for KS type 1 (Fig. 3A). Specifically, we address the formation and function of synapses to gain mechanistic insights into the pathogenic neurodevelopment leading to intellectual disability in KS patients. The recurring detection of increased inhibitory synapse formation and altered neuronal communication in all three model systems (mouse KS type 1, human KS type 1, and human KS type 2) is a central theme. Aberrant synapse formation and function are key drivers of neurodevelopmental disorders with intellectual disability (Batool et al., 2019; Lepeta et al., 2016; Parenti et al., 2020; Washbourne, 2015). Here, we demonstrate a novel imbalance between excitatory and inhibitory synaptic formation and function in KS models. This imbalance is caused by increases in the number of inhibitory synapses,

as shown by elevated synaptic puncta metrics of vGAT and Gephyrin in cultured neurons (Fig. 1C, 1D, 2D, 2E, 3G, 3H, 3M, 3N) as well as elevated vGAT in immunohistology of mouse brain slices (Fig. 5A-C). *In vitro* the overall number of synapses was increased in mutant neurons (as shown by signals for synapsin and bassoon – two presynaptic markers found in inhibitory and excitatory neurons, Fig. 3C-F), explained by gain of inhibitory synapses, and increased inhibition in neural networks shown in hippocampal slice recordings (Fig. 5 F-H) or calcium imaging of purely inhibitory neurons (Suppl. Fig. 2). This is not correlated with an increase in the number of inhibitory neurons but an increase of inhibitory synapses per neuron in mouse cultures (Fig. 4D-G), while the total number of hippocampal neurons was reduced (Fig. 4A-C). This finding of increased synapse formation (vs. increased number of inhibitory cells) also applies to human neurons, which are produced by transducing and plating the same number of iPSCs per genetic condition (Cre vs. ΔCre) in a standardized manner, leading to the same number of neurons. Additionally, we detected decreased puncta metrics for presynaptic vGluT1 or postsynaptic PSD95 (Fig. 1C, 1D, 3I, 3J), possibly inferring a reduction and altered morphology of excitatory synapses, correlating with decreased human excitatory or mouse hippocampal (glutamatergic and GABAergic) neuronal communication (Fig. 1G-K, 2G-K, 4H-L). These data suggest that the KS mutations change the overall development of synapses and skew the balance toward inhibitory synaptic dominance.

The molecular basis of the observed synaptic changes in KS are likely rooted in the chromatin remodeling functions of both KMT2D and KDM6A. Mutations in *KMT2D* are known to disrupt histone methylation, altering gene expression (Dhar and Lee, 2021; Jung et al., 2023; Zhang et al., 2015). Our results suggest that *KMT2D* and *KDM6A* loss-of-function mutations may lead to the repression of transcriptional programs necessary for maintaining a balanced level of excitatory and inhibitory synapses. Restoration of excitatory and inhibitory synaptic balance presents a promising therapeutic strategy for KS. In particular, pharmacological interventions that increase excitatory synaptic activity or decrease excessive inhibitory synaptic activity could help to rescue synaptic homeostasis. Several drugs which have been shown to enhance AMPA (Aniracetam, Piracetam) and NMDA (D-cycloserine) receptor activity as well as those shown to decrease GABA-A (Bicuculline, Gabazine) or GABA-B (CGP55845) receptor activity would serve as initial tools for studies involving the pharmacological modulation of the I/E imbalance and for determining potential targets in treating Kabuki syndrome. Interestingly, previous research on the KS-related disorder Rubinstein-Taybi syndrome has uncovered evidence of altered neural development and consequential synaptic plasticity deficits (Alarcón et al., 2004; de Thonel et al., 2022; Lintas and Persico, 2018).

In summary, our results suggest that KS type 1- and KS type 2-causing mutations enhance inhibitory synaptic transmission while reducing excitatory synaptic transmission, and the resulting imbalance in neuronal inhibition to excitation represses information flow and coordinated network activity (Fig. 6). This conclusion is supported by morphological and functional changes, including changes in the number of synapses, changes synaptic transmission, and alterations in calcium event frequency. The combined increase in

inhibitory synaptic markers and decrease in excitatory synaptic markers, coupled with alterations in synaptic currents and calcium activity, suggest that aberrant synaptic function is the underlying cause for the intellectual disability associated with KS. Ultimately, our findings lay the foundation for development of treatments designed to target the synaptic basis of intellectual disability in KS and potentially other similar disorders. At the same time, our results suggest that inhibiting *KMT2D* and *KDM6A* may promote inhibitory synapse formation.

MATERIALS AND METHODS

Mice: Animal experiments conducted in this study were in accordance with National Institute of Health Guidelines for the Care and Use of Laboratory Mice and approved by the Institutional Animal Care and Use Committee (IACUC) at the University of Notre Dame. The Kmt2d+/βGeo mice used in this study were originally generated at Bay Genomics and then back-crossed for several generations to obtain line stability. An expression cassette encoding a β-galactosidase neomycin resistance fusion protein (βGeo) was inserted into intron 50 of *Kmt2d* on mouse chromosome 15 and is predicted to generate a truncated Kmt2d protein with peptide sequence corresponding to the first 50 exons of *Kmt2d* fused to βGeo, but lacking the SET domain and therefore methyltransferase activity (Bjornsson et al., 2014). For breeding of Kmt2d+/βGeo mice, matings were set up using a heterozygous male and WT female. For all analyses, littermates were used.

Mouse hippocampal cultures: To generate cultured mouse hippocampal neurons, brains were dissected from P0 mice and rinsed quickly with ice-cold Hank's Balanced Buffered Saline (HBSS) before continued dissection of the hippocampus, digestion with papain, and then seeding onto matrigel-coated coverslips in MEM medium (ThermoFisher Scientific). P0 was defined as the day the pups were born. On day in vitro (DIV) 1, the medium was changed to neurobasal medium containing B27. On DIV3, the medium was exchanged for medium containing 2 μM AraC, and cells were infected with lentiviruses that encoded GCaMP8m. Calcium imaging or immunostaining was performed at DIV14–16, when the cells are considered mature.

Immunofluorescent labeling of hippocampus: For immunohistochemistry, P30 mice were perfused with phosphate-buffered saline (PBS) and then PBS containing 4% PFA. Brains were dissected and rinsed quickly in ice-cold PBS before soaking in 30% sucrose. Brain tissues were embedded in optimal cutting temperature compound (OCT, Tissue Plus, Fisher) with embedding mold and frozen on dry ice. Embedded brain samples were stored at −80°C until further use. To sample the hippocampus in horizontal planes, multiple dorsal-ventral (horizontal) cryosections with a thickness of 30 um were collected. Brain sections were sliced using a cryostat (Leica Microsystems, CM3050-S) and then blocked using a solution containing goat serum and Triton-X100. Immunostaining was performed

on slices while free-floating. Individual slices were mounted manually onto superfrost slides (VWR) using a paint brush.

Calcium imaging: Calcium imaging was performed as previously described (Patzke et al., 2021; Sun and Südhof, 2021). Coverslips were gently placed into a dark imaging chamber with an open bottom and then washed twice with a washing buffer before time-lapse imaging was performed in calcium-imaging buffer. After 1–2 min equilibration in a 37°C incubator, calcium-imaging was performed on an inverted epi-fluorescence microscope (Nikon EclipseTS2R) with a 488 nm filter at room temperature. GCaMP8m fluorescence was recorded for 2 min at a frame rate of 9-10 frames/s. Approximately 1000-3000 time-lapse images were acquired at a 1 × digital zoom using a 20x objective. For each condition, 4-5 fields of view were imaged per coverslip and a minimal 2 coverslips were used for each biological batch. All images were acquired using the same exposure time. Time-lapse imaging was performed in areas containing confluent neuron populations with few overlapping cell somata.

Hippocampal slice electrophysiology: Mice were anesthetized with isoflurane followed by ketamine/xylazine, then rapid cardiac perfusion was performed using ice-cold sucrose artificial cerebrospinal fluid (ACSF) containing the following (in mM): 85 NaCl, 2.5 KCl, 1.25 NaH2PO4, 25 NaHCO3, 25 glucose, 75 sucrose, 0.5 CaCl2, and 4 MgCl2, equilibrated with 95% O2/5% CO2 before mice were decapitated. Brains were rapidly removed and placed in the same ice-cold sucrose ACSF as described previously (Nomura et al., 2023). Horizontal hippocampal slices (250 µm thick) were prepared using a Leica VT1000S or VT1200 S vibratome and transferred to a heated (28-32°C) holding chamber containing the same sucrose ACSF, which was gradually exchanged for regular ACSF containing the following (in mM): 125 NaCl, 2.5 KCl, 1.25 NaH2PO4, 25 NaHCO3, 25 glucose, 2 CaCl2, and 1 MgCl2, equilibrated with 95% O2/5% CO2 at room temperature. After incubation in regular ACSF for at least one hour, slices were transferred to a recording chamber and perfused continuously with oxygenated regular ACSF at a flow rate of 2 ml/min.

Excitatory and inhibitory postsynaptic currents (EPSCs and IPSCs) were recorded from pyramidal neurons in the CA1 subregion of the hippocampus. Stimulating electrodes were placed in the stratum radiatum to stimulate Schaffer collaterals from the CA3 neurons. EPSCs and IPSCs were isolated by switching the holding voltage at -50 mV and at 0 mV, which are close to the reversal potentials for Cl- and Na+ (Kourdougli et al., 2024). Stimulation intensity was adjusted to evoke EPSCs with amplitudes of 300- 400 pA in individual neurons, and then IPSCs were recorded from the same neurons. The ratio of IPSC amplitude to EPSC amplitude (I to E ratio) was measured in each cell and was compared between genotypes (WT and Het).

Viral constructs. The following lentiviral constructs were used: 1. FUW-TetO-Ngn2-T2A-puromycin (TetO promoter drives expression of full-length mouse Ngn2 and of puromycin via the cleavage-peptide sequence T2A). 2. FUW-rtTA. 3. FUW-GFP::Cre to express Cre-recombinase or GFP::ΔCre for the wild-type control. 6. FUW-GCaMP8m for Ca^{2+} imaging.

Virus generation. Lentiviruses were produced as described (Zhang et al., 2013) in HEK293T cells (ATCC, VA) by co-transfection with three helper plasmids (pRSV-REV, pMDLg/pRRE and vesicular stomatitis virus G protein expression vector) with 12 µg of lentiviral vector DNA and 6 µg of each of the helper plasmid DNA per 75 cm^2 culture area) using calcium phosphate. Lentiviruses were harvested in the medium 48 h after transfection, aliquoted, and frozen at -80ºC.

Cell culture. Experiments were performed as follows. 1019 iPSCs (ATCC-DYS0100 Human Induced Pluripotent Stem (IPS) Cells) were maintained as feeder-free cells in Stemflex medium (Thermo). Mouse glial cells were cultured from the forebrain of new-born wild-type CD1 mice. Briefly, new-born mouse forebrain homogenates were digested with papain and EDTA for 15 min, cells were dissociated by harsh trituration to avoid growing of neurons, and plated onto T75 flasks in DMEM supplemented with 10% FBS. Upon reaching confluence, glial cells were trypsinized and replated at lower density a total of two times to remove potential trace amounts of mouse neurons before the glia cell cultures were used for co-culture experiment with human neurons.

Standard protocol for generation of neurons from conditional mutant human iPS cells and for activating the conditional mutations. Human neuron generation has been described previously (Zhang et al., 2013). Briefly, targeted human iPSCs were treated with Accutase (Innovative Cell Technologies) and plated as dissociated cells in 24-well plates (1 x 10^4 cells/well) on day -1. Cells were plated on matrigel (BD Biosciences)-coated coverslips in Stemflex containing 2 mM thiazovivin (Bio Vision). At the same time point, lentiviruses were prepared as described above and added to each well (14 µl/well of 24-well plate) in a total volume of 500 µl. Mainly two different types of lentiviruses were used for co-infection: the lentiviruses used for human neuron induction as described, and lentiviruses expressing either Cre-recombinase (to create a null allele) under control of the ubiquitin promoter or an inactive mutated ΔCre-recombinase for the wild-type control. On day 0, the culture medium was replaced with N2/DMEM/F12/NEAA (Invitrogen) containing human BDNF (10 ng/ml, PeproTech), human NT-3 (10 ng/ml, PeproTech), and mouse Laminin-1 (0.2 µg/ml, Invitrogen). Doxycycline (2 µg/ml, Clontech) was added on day 0 to induce TetO gene expression and retained in the medium until the end of the experiment. On day 1, a 24 hr puromycin selection (1 µg/ml) period was started. On day 2, mouse glia cells were added in neurobasal medium supplemented with B27/Glutamax (Invitrogen) containing BDNF, NT3 and Laminin-1; Ara-C (2 µM, Sigma) was added to the medium to inhibit glial proliferation. After day 2, 50% of the medium in each well was exchanged every 2 days. FBS (5%) was added to the culture medium on day 10 to support astrocyte viability, and human neurons were assayed after at least 2 (excitatory) or 4 (inhibitory) months or as indicated.

Data presentation and statistics. Part of Figures 3B, 5F, and 6, were created with BioRender.com. All data shown are individual values and means ± SEMs; Number of measured cells and/or independent experiments is indicated inside each bar or mentioned in the figure. All statistical analyses were performed using r unpaired two-tailed Student's t-test (when two experimental were compared to each other) comparing the test sample to the control sample examined in the same experiments. No power analysis were performed to predetermine sample sizes. Our sample sizes are similar to those generally employed in the field. Sample allocation was random. We did not test for normal distribution.

AKNOWLEDGEMENTS

This work was supported by funds from the University of Notre, the Brain foundation to C.P. We thank Dr. Kasturi Haldar for sharing the Kmt2d+/βGeo mice with us. We thank the undergraduate summer students Isabella Wiebelt-Smith and Jeremiah Lopez for helping with the synapse binning experiment and counting neurons.

CONFLICT OF INTEREST

The authors declare no competing financial interests.

AUTHOR CONTRIBUTIONS

C.P. conceived the study. C.P. and J.K., designed most of the experiments. J.K., A.W., S.M., A.W., J.S., A.N., K.H., J.B.-P., and S.N. performed and analyzed most of the experiments. T.N., and A.C. contributed to specific experiments. C.P. and J.K. prepared the manuscript with input from all authors.

REFERENCES

Agger, K., Cloos, P.A., Christensen, J., Pasini, D., Rose, S., Rappsilber, J., Issaeva, I., Canaani, E., Salcini, A.E., and Helin, K. (2007). UTX and JMJD3 are histone H3K27 demethylases involved in HOX gene regulation and development. Nature *449*, 731-734.

Alarcón, J.M., Malleret, G., Touzani, K., Vronskaya, S., Ishii, S., Kandel, E.R., and Barco, A. (2004). Chromatin Acetylation, Memory, and LTP Are Impaired in CBP+/− Mice: A Model for the Cognitive Deficit in Rubinstein-Taybi Syndrome and Its Amelioration. Neuron *42*, 947-959.

Barry, K.K., Tsaparlis, M., Hoffman, D., Hartman, D., Adam, M.P., Hung, C., and Bodamer, O.A. (2022). From Genotype to Phenotype-A Review of Kabuki Syndrome. Genes (Basel) *13*.

Batool, S., Raza, H., Zaidi, J., Riaz, S., Hasan, S., and Syed, N.I. (2019). Synapse formation: from cellular and molecular mechanisms to neurodevelopmental and neurodegenerative disorders. Journal of neurophysiology *121*, 1381-1397.

Benjamin, J.S., Pilarowski, G.O., Carosso, G.A., Zhang, L., Huso, D.L., Goff, L.A., Vernon, H.J., Hansen, K.D., and Bjornsson, H.T. (2017). A ketogenic diet rescues hippocampal memory defects in a mouse model of Kabuki syndrome. Proceedings of the National Academy of Sciences *114*, 125-130.

Bjornsson, H.T., Benjamin, J.S., Zhang, L., Weissman, J., Gerber, E.E., Chen, Y.C., Vaurio, R.G., Potter, M.C., Hansen, K.D., and Dietz, H.C. (2014). Histone deacetylase inhibition rescues structural and functional brain deficits in a mouse model of Kabuki syndrome. Science translational medicine *6*, 256ra135.

Bögershausen, N., and Wollnik, B. (2013). Unmasking Kabuki syndrome. Clin Genet *83*, 201-211.

Boniel, S., Szymańska, K., Śmigiel, R., and Szczałuba, K. (2021). Kabuki Syndrome-Clinical Review with Molecular Aspects. Genes (Basel) *12*.

Carosso, G.A., Boukas, L., Augustin, J.J., Nguyen, H.N., Winer, B.L., Cannon, G.H., Robertson, J.D., Zhang, L., Hansen, K.D., Goff, L.A.*, et al.* (2019). Precocious neuronal differentiation and disrupted oxygen responses in Kabuki syndrome. JCI Insight *4*.

de Thonel, A., Ahlskog, J.K., Daupin, K., Dubreuil, V., Berthelet, J., Chaput, C., Pires, G., Leonetti, C., Abane, R., Barris, L.C.*, et al.* (2022). CBP-HSF2 structural and functional interplay in Rubinstein-Taybi neurodevelopmental disorder. Nature communications *13*, 7002.

Dhar, S.S., and Lee, M.G. (2021). Cancer-epigenetic function of the histone methyltransferase KMT2D and therapeutic opportunities for the treatment of KMT2D-deficient tumors. Oncotarget *12*, 1296-1308.

Dhar, S.S., Lee, S.H., Kan, P.Y., Voigt, P., Ma, L., Shi, X., Reinberg, D., and Lee, M.G. (2012). Trans-tail regulation of MLL4-catalyzed H3K4 methylation by H4R3 symmetric dimethylation is mediated by a tandem PHD of MLL4. Genes Dev *26*, 2749-2762.

Egolf, S., Zou, J., Anderson, A., Simpson, C.L., Aubert, Y., Prouty, S., Ge, K., Seykora, J.T., and Capell, B.C. (2021). MLL4 mediates differentiation and tumor suppression through ferroptosis. Sci Adv *7*, eabj9141.

Gao, C.W., Lin, W., Riddle, R.C., Chopra, S., Kim, J., Boukas, L., Hansen, K.D., Björnsson, H.T., and Fahrner, J.A. (2024). Growth deficiency in a mouse model of

Kabuki syndrome 2 bears mechanistic similarities to Kabuki syndrome 1. PLoS genetics *20*, e1011310.

Greenfield, A., Carrel, L., Pennisi, D., Philippe, C., Quaderi, N., Siggers, P., Steiner, K., Tam, P.P., Monaco, A.P., Willard, H.F.*, et al.* (1998). The UTX gene escapes X inactivation in mice and humans. Human molecular genetics *7*, 737-742.

Hannibal, M.C., Buckingham, K.J., Ng, S.B., Ming, J.E., Beck, A.E., McMillin, M.J., Gildersleeve, H.I., Bigham, A.W., Tabor, H.K., Mefford, H.C.*, et al.* (2011). Spectrum of MLL2 (ALR) mutations in 110 cases of Kabuki syndrome. American journal of medical genetics Part A *155a*, 1511-1516.

Hong, S., Cho, Y.W., Yu, L.R., Yu, H., Veenstra, T.D., and Ge, K. (2007). Identification of JmjC domain-containing UTX and JMJD3 as histone H3 lysine 27 demethylases. Proceedings of the National Academy of Sciences of the United States of America *104*, 18439-18444.

Jung, Y.L., Hung, C., Choi, J., Lee, E.A., and Bodamer, O. (2023). Characterizing the molecular impact of KMT2D variants on the epigenetic and transcriptional landscapes in Kabuki syndrome. Human molecular genetics *32*, 2251-2261.

Kourdougli, N., Nomura, T., Wu, M.W., Heuvelmans, A., Dobler, Z., Contractor, A., and Portera-Cailliau, C. (2024). The NKCC1 Inhibitor Bumetanide Restores Cortical Feedforward Inhibition and Lessens Sensory Hypersensitivity in Early Postnatal Fragile X Mice. Biological psychiatry.

Lan, F., Bayliss, P.E., Rinn, J.L., Whetstine, J.R., Wang, J.K., Chen, S., Iwase, S., Alpatov, R., Issaeva, I., Canaani, E.*, et al.* (2007). A histone H3 lysine 27 demethylase regulates animal posterior development. Nature *449*, 689-694.

Lawrence, M.S., Stojanov, P., Mermel, C.H., Robinson, J.T., Garraway, L.A., Golub, T.R., Meyerson, M., Gabriel, S.B., Lander, E.S., and Getz, G. (2014). Discovery and saturation analysis of cancer genes across 21 tumour types. Nature *505*, 495-501.

Lee, J.E., Wang, C., Xu, S., Cho, Y.W., Wang, L., Feng, X., Baldridge, A., Sartorelli, V., Zhuang, L., Peng, W.*, et al.* (2013). H3K4 mono- and di-methyltransferase MLL4 is required for enhancer activation during cell differentiation. Elife *2*, e01503.

Lepeta, K., Lourenco, M.V., Schweitzer, B.C., Martino Adami, P.V., Banerjee, P., Catuara-Solarz, S., de La Fuente Revenga, M., Guillem, A.M., Haidar, M., Ijomone, O.M.*, et al.* (2016). Synaptopathies: synaptic dysfunction in neurological disorders - A review from students to students. Journal of neurochemistry *138*, 785-805.

Li, Y., Bögershausen, N., Alanay, Y., Simsek Kiper, P.O., Plume, N., Keupp, K., Pohl, E., Pawlik, B., Rachwalski, M., Milz, E.*, et al.* (2011). A mutation screen in patients with Kabuki syndrome. Hum Genet *130*, 715-724.

Lintas, C., and Persico, A.M. (2018). Unraveling molecular pathways shared by Kabuki and Kabuki-like syndromes. Clin Genet *94*, 283-295.

Marcó de la Cruz, B., Campos, J., Molinaro, A., Xie, X., Jin, G., Wei, Z., Acuna, C., and Sterky, F.H. (2024). Liprin-α proteins are master regulators of human presynapse assembly. Nature neuroscience *27*, 629-642.

Miyake, N., Mizuno, S., Okamoto, N., Ohashi, H., Shiina, M., Ogata, K., Tsurusaki, Y., Nakashima, M., Saitsu, H., Niikawa, N.*, et al.* (2013). KDM6A point mutations cause Kabuki syndrome. Human mutation *34*, 108-110.

Ng, S.B., Bigham, A.W., Buckingham, K.J., Hannibal, M.C., McMillin, M.J., Gildersleeve, H.I., Beck, A.E., Tabor, H.K., Cooper, G.M., Mefford, H.C.*, et al.* (2010). Exome sequencing identifies MLL2 mutations as a cause of Kabuki syndrome. Nature genetics *42*, 790-793.

Niikawa, N., Kuroki, Y., Kajii, T., Matsuura, N., Ishikiriyama, S., Tonoki, H., Ishikawa, N., Yamada, Y., Fujita, M., Umemoto, H.*, et al.* (1988). Kabuki make-up (Niikawa-Kuroki) syndrome: a study of 62 patients. Am J Med Genet *31*, 565-589.

Nomura, T., Taniguchi, S., Wang, Y.Z., Yeh, N.H., Wilen, A.P., Castillon, C.C.M., Foote, K.M., Xu, J., Armstrong, J.N., Savas, J.N.*, et al.* (2023). A Pathogenic Missense Mutation in Kainate Receptors Elevates Dendritic Excitability and Synaptic Integration through Dysregulation of SK Channels. The Journal of neuroscience : the official journal of the Society for Neuroscience *43*, 7913-7928.

Parenti, I., Rabaneda, L.G., Schoen, H., and Novarino, G. (2020). Neurodevelopmental Disorders: From Genetics to Functional Pathways. Trends in Neurosciences *43*, 608-621.

Park, Y.K., Lee, J.E., Yan, Z., McKernan, K., O'Haren, T., Wang, W., Peng, W., and Ge, K. (2021). Interplay of BAF and MLL4 promotes cell type-specific enhancer activation. Nature communications *12*, 1630.

Patzke, C., Brockmann, M.M., Dai, J., Gan, K.J., Grauel, M.K., Fenske, P., Liu, Y., Acuna, C., Rosenmund, C., and Sudhof, T.C. (2019). Neuromodulator Signaling Bidirectionally Controls Vesicle Numbers in Human Synapses. Cell *179*, 498-513 e422.

Patzke, C., Dai, J., Brockmann, M.M., Sun, Z., Fenske, P., Rosenmund, C., and Südhof, T.C. (2021). Cannabinoid receptor activation acutely increases synaptic vesicle numbers by activating synapsins in human synapses. Molecular psychiatry.

Patzke, C., and Südhof, T.C. (2016). The conditional KO approach: Cre/Lox technology in human neurons. Rare Dis *4*, e1131884.

Paulussen, A.D., Stegmann, A.P., Blok, M.J., Tserpelis, D., Posma-Velter, C., Detisch, Y., Smeets, E.E., Wagemans, A., Schrander, J.J., van den Boogaard, M.J.*, et al.*

(2011). MLL2 mutation spectrum in 45 patients with Kabuki syndrome. Human mutation *32*, E2018-2025.

Schwenty-Lara, J., Nehl, D., and Borchers, A. (2020). The histone methyltransferase KMT2D, mutated in Kabuki syndrome patients, is required for neural crest cell formation and migration. Human molecular genetics *29*, 305-319.

Srivastava, A.K., and Schwartz, C.E. (2014). Intellectual disability and autism spectrum disorders: causal genes and molecular mechanisms. Neurosci Biobehav Rev *46 Pt 2*, 161-174.

Sullivan, P.F., and Geschwind, D.H. (2019). Defining the Genetic, Genomic, Cellular, and Diagnostic Architectures of Psychiatric Disorders. Cell *177*, 162-183.

Sun, Z., and Südhof, T.C. (2021). A simple Ca(2+)-imaging approach to neural network analyses in cultured neurons. Journal of neuroscience methods *349*, 109041.

Van, H.T., Xie, G., Dong, P., Liu, Z., and Ge, K. (2024). KMT2 Family of H3K4 Methyltransferases: Enzymatic Activity-dependent and -independent Functions. J Mol Biol *436*, 168453.

Van Laarhoven, P.M., Neitzel, L.R., Quintana, A.M., Geiger, E.A., Zackai, E.H., Clouthier, D.E., Artinger, K.B., Ming, J.E., and Shaikh, T.H. (2015). Kabuki syndrome genes KMT2D and KDM6A: functional analyses demonstrate critical roles in craniofacial, heart and brain development. Human molecular genetics *24*, 4443-4453.

Walport, L.J., Hopkinson, R.J., Vollmar, M., Madden, S.K., Gileadi, C., Oppermann, U., Schofield, C.J., and Johansson, C. (2014). Human UTY(KDM6C) is a male-specific Nϵ-methyl lysyl demethylase. The Journal of biological chemistry *289*, 18302-18313.

Washbourne, P. (2015). Synapse assembly and neurodevelopmental disorders. Neuropsychopharmacology *40*, 4-15.

Wu, Q., Tian, Y., Zhang, J., Tong, X., Huang, H., Li, S., Zhao, H., Tang, Y., Yuan, C., Wang, K.*, et al.* (2018). In vivo CRISPR screening unveils histone demethylase UTX as an important epigenetic regulator in lung tumorigenesis. Proceedings of the National Academy of Sciences of the United States of America *115*, E3978-e3986.

Yang, N., Zuchero, J.B., Ahlenius, H., Marro, S., Ng, Y.H., Vierbuchen, T., Hawkins, J.S., Geissler, R., Barres, B.A., and Wernig, M. (2013). Generation of oligodendroglial cells by direct lineage conversion. Nature biotechnology *31*, 434-439.

Zhang, J., Dominguez-Sola, D., Hussein, S., Lee, J.E., Holmes, A.B., Bansal, M., Vlasevska, S., Mo, T., Tang, H., Basso, K.*, et al.* (2015). Disruption of KMT2D perturbs germinal center B cell development and promotes lymphomagenesis. Nat Med *21*, 1190-1198.

Zhang, Y., Pak, C., Han, Y., Ahlenius, H., Zhang, Z., Chanda, S., Marro, S., Patzke, C., Acuna, C., Covy, J.*, et al.* (2013). Rapid Single-Step Induction of Functional Neurons from Human Pluripotent Stem Cells. Neuron *78*, 785-798.

Zoghbi, H.Y., and Bear, M.F. (2012). Synaptic dysfunction in neurodevelopmental disorders associated with autism and intellectual disabilities. Cold Spring Harbor perspectives in biology *4*.

FIGURES AND FIGURE LEGENDS

Fig.1

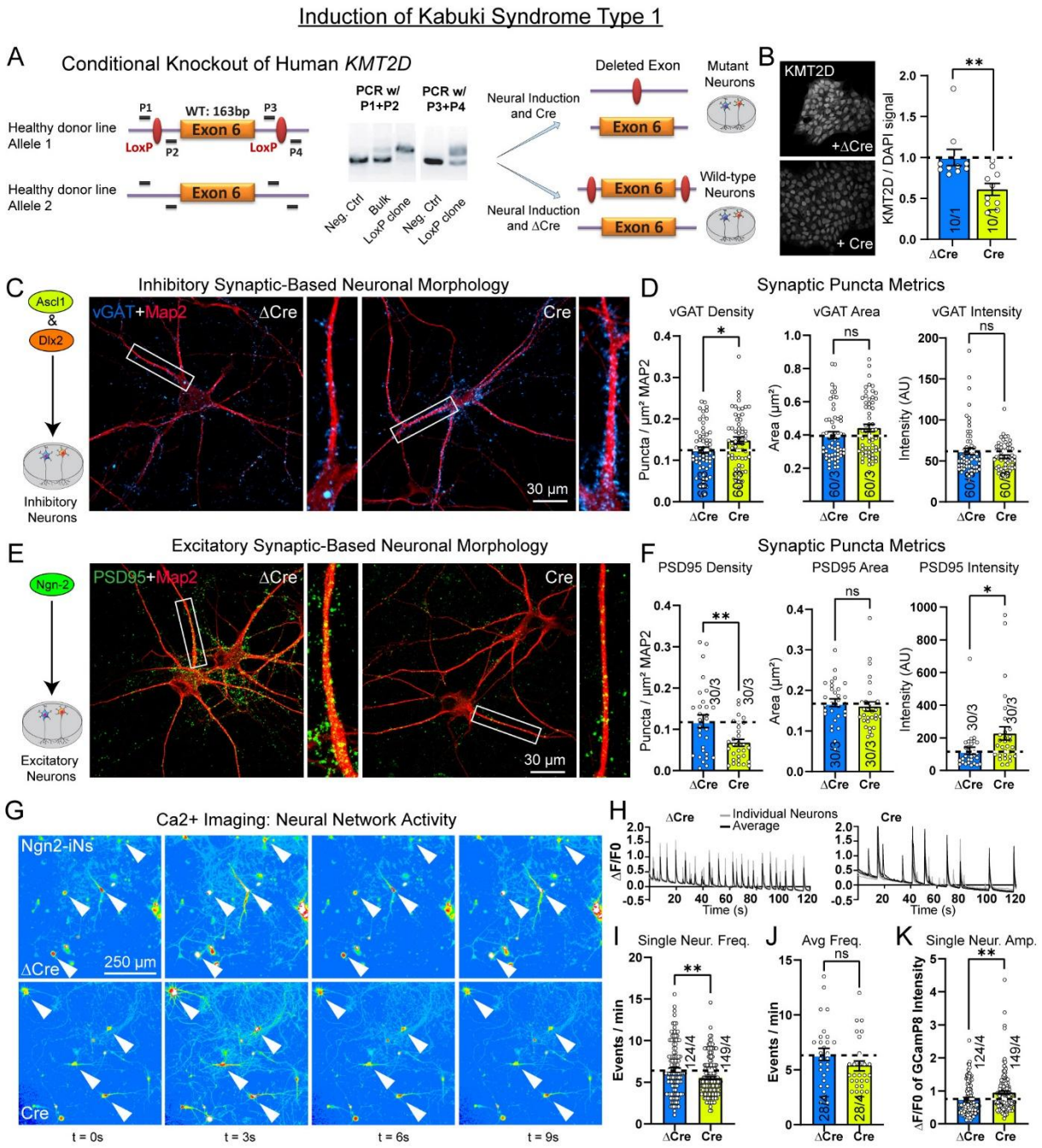

Figure 1: Increased synaptic inhibition and decreased excitation in a human model for Kabuki syndrome type 1

A, General strategy for Cre/loxP-mediated induction of Kabuki syndrome type1 in human iPSCs from a donor without disease-causing mutations, and their differentiation into purely isogenic wild-type and mutant induced neurons (iNs). Specific heterozygous targeting of *KMT2D* and PCR-based screening strategy for correctly inserted loxP sites, using primers P1+P2 for the upstream and P3+P4 for the downstream loxP site.

B, Immunofluorescent signal by anti KMT2D. Expression of active Cre resulted in ~40% decrease of KMT2D protein as measured by fluorescent immunocytochemistry, compared to iPSCs treated with inactive ΔCre.

C and D, GABAergic (generated by overexpression of Ascl1 and Dlx2 in iPSCs) *KMT2D*-mutant neurons (Cre) inhibitory neurons exhibit an increase in vGAT synaptic puncta density at 4 months.

E and F, Glutamatergic (generated by overexpression of Ngn2) *KMT2D*-mutant (Cre) excitatory neurons show a decrease in PSD95 synaptic puncta density at 2 months.

G, Representative calcium imaging micrographs of cultured wild-type (ΔCre) and mutant (Cre) excitatory human neurons overexpressing GCaMP8. Neuronal activity was induced by 2.5 mM KCl and 2 mM $CaCl_2$. Warmer colors indicate higher fluorescence intensity. Arrows highlight active neurons displaying calcium transients.

H, Representative traces of GCamp8 transients showing fluorescence intensity changes ($\Delta F/F_0$) over time. Mutant neurons show decreased event frequency.

I-K, Summary graphs of individual neuron firing frequency (I), average firing frequency per view field (J), and signal intensities in single neurons (K).

Data are individual values (one image or video in B, D, F, J; and one cell in I and K) and means ± SEM; statistical significance was assessed by two-tailed unpaired Student's t-test (*, $p<0.05$; ** $p<0.01$).

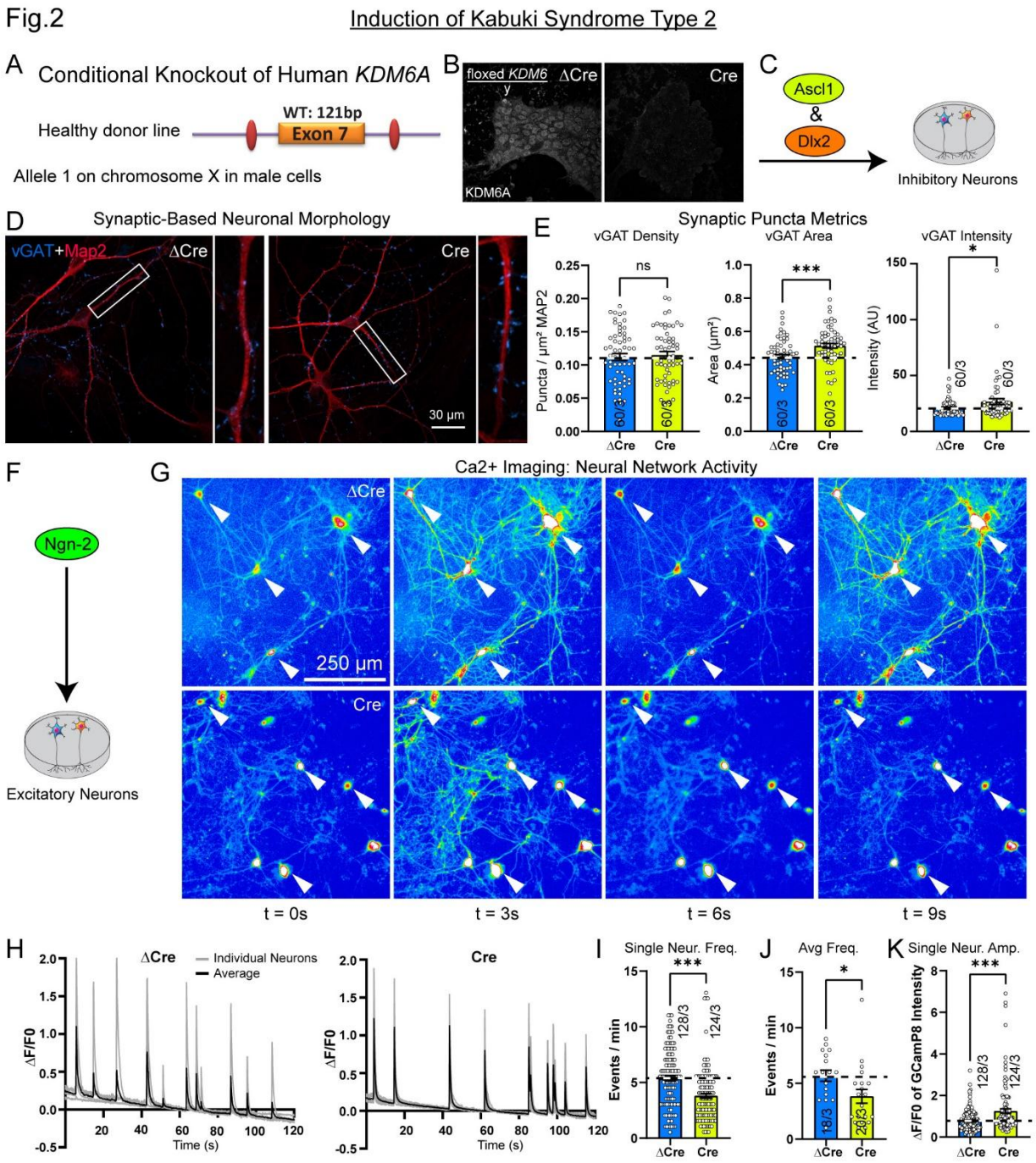

Figure 2: Increased inhibitory synapse development in a human model for Kabuki syndrome type 2

A, Specific hemizygous targeting strategy of X-linked *KDM6A* (also called *UTX*) in iPSCs from a male donor without disease-causing mutations.

B, Expression of active Cre results in loss of KDM6A signal, as measured by fluorescent immunocytochemistry, compared to iPSCs treated with inactive ΔCre.

C-E, Differentiation protocols used for generating GABAergic iNs (overexpression of transcription factors Ascl1 and Dlx2) for subsequent synapse analysis. *KDM6A*-Mutant (Cre) inhibitory neurons show an increase in vGAT synaptic puncta area and intensity (E) at 4 months.

F and G, Differentiation protocols used for generating glutamatergic iNs (overexpression of transcription factor Ngn2) for subsequent calcium imaging at 2 months. Representative calcium imaging micrographs of wild-type (ΔCre) and mutant (Cre) human iNs overexpressing GCaMP8. Neuronal activity was induced by 8 mM KCl and 4 mM $CaCl_2$. Warmer colors indicate higher fluorescence intensity. Arrows point to active neurons displaying calcium transients.

H, Representative traces of GCaMP8m transients showing fluorescence intensity changes ($\Delta F/F_0$) over time. Mutant neurons show decreased event frequency.

I-K, Summary graphs of individual neuron firing frequency (H), average firing frequency per view field (I), and signal intensities in single neurons (J).

Data are presented as individual values (one image or video in E and I; and one cell in H and J) and means ± SEM; statistical significance was assessed by two-tailed unpaired Student's t-test (*, $p<0.05$; *** $p<0.001$).

Fig.3

Mouse model for Kabuki Syndrome Type 1

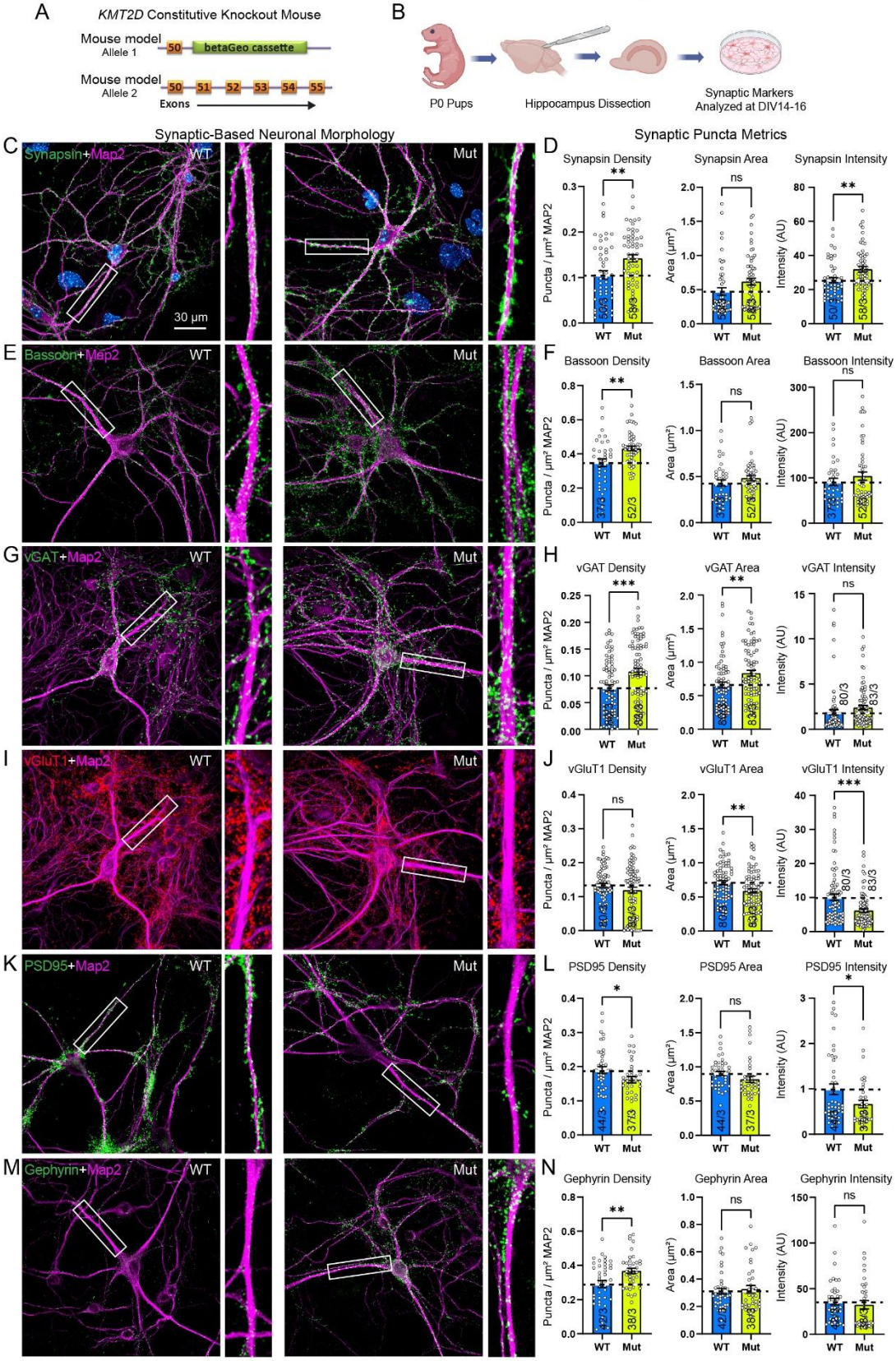

Figure 3: Increased development of inhibitory synapses in a mouse model for Kabuki syndrome type 1

A and B, Schematic rationale of experiments: Newborn P0 mouse pups (littermates with (Mut) and without (WT) heterozygous mutation) were used to analyze synaptic puncta metrics in cultured hippocampal cells.

C and D, Immunocytochemistry images showing synaptic morphology labeled for presynaptic Synapsin-1 (green), Map2 (magenta), and DAPI (blue). A zoomed-in view is included. Summary graphs show synaptic puncta density, puncta area and intensity for Synapsins-1.

E and F, Immunocytochemistry images showing synaptic morphology labeled for presynaptic Bassoon (green), Map2 (magenta), and DAPI (blue). A zoomed-in view is included. Summary graphs show synaptic puncta densities, puncta area and intensities for Bassoon.

G - I, Immunocytochemistry images of the same cells showing synaptic morphology of presynaptic excitatory vGluT1 (G) and inhibitory vGAT (I) synapses. H and J, Summary graphs show synaptic puncta density, puncta area and intensity.

K and L, Immunocytochemistry images showing synaptic morphology labeled for postsynaptic excitatory PSD95 (green), Map2 (magenta), and DAPI (blue). A zoomed-in view is included. Summary graphs show synaptic puncta densities, puncta area and intensities for PSD95.

M and N, Immunocytochemistry images showing synaptic-based morphology labeled for postsynaptic inhibitory Gephyrin (green), Map2 (magenta), and DAPI (blue). A zoomed-in view is included. Summary graphs show synaptic puncta densities, puncta area and intensities for Gephyrin.

Data are presented as individual values (each representing one image) and means ± SEM; statistical significance was assessed by two-tailed unpaired Student's t-test (*, $p<0.05$; **, $p<0.01$; *** $p<0.001$).

Fig.4

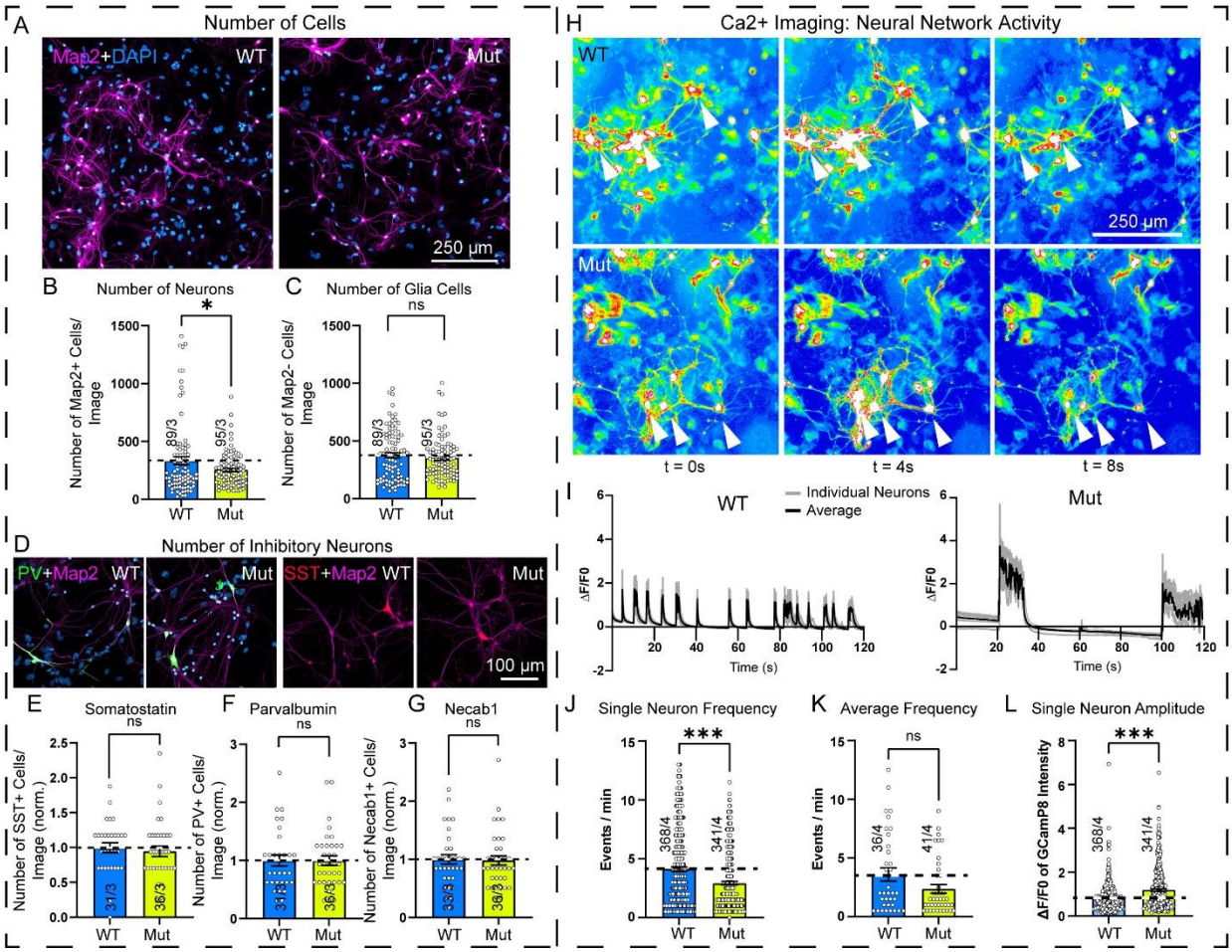

Figure 4. Kmt2d mutation in mice leads to decreased neuronal calcium activity but no change in the number of inhibitory neurons.

A-C, Representative micrographs of WT and Mut hippocampal cells. Neuronal numbers were assessed by Map2-positive somata. Map2-negative cells were considered glia cells.

D-G, Representative micrographs showing WT and Mut hippocampal cells stained for inhibitory neuronal markers Somatostatin (SST) and Parvalbumin (PV). Summary graphs quantify the relative (to WT) number of positive cells, including the inhibitory neuronal marker Necab1.

H, Representative calcium imaging micrographs of cultured wild-type (WT) and mutant (Mut) mouse hippocampal neurons overexpressing GCaMP8m. Network activity was induced with 2.5 mM KCl and 2 mM $CaCl_2$. Warmer colors indicate higher fluorescence intensity. Arrows highlight active neurons showing calcium transients.

I, Representative traces of GCaMPm8 transients. Fluorescence intensity changes (ΔF/F0) over time reveal a more clustered pattern and higher signal intensities in Mut neurons.

J-L, Summary graphs showing individual neuron firing frequency (J), average firing frequency per view field (K), and signal intensities in single neurons (L).

Data are presented as individual values (one movie or image in B, C, E, F, G, K; and one cell in J and L) and means ± SEM; statistical significance was assessed by two-tailed unpaired Student's t-test (*, $p<0.05$; *** $p<0.001$).

Fig.5

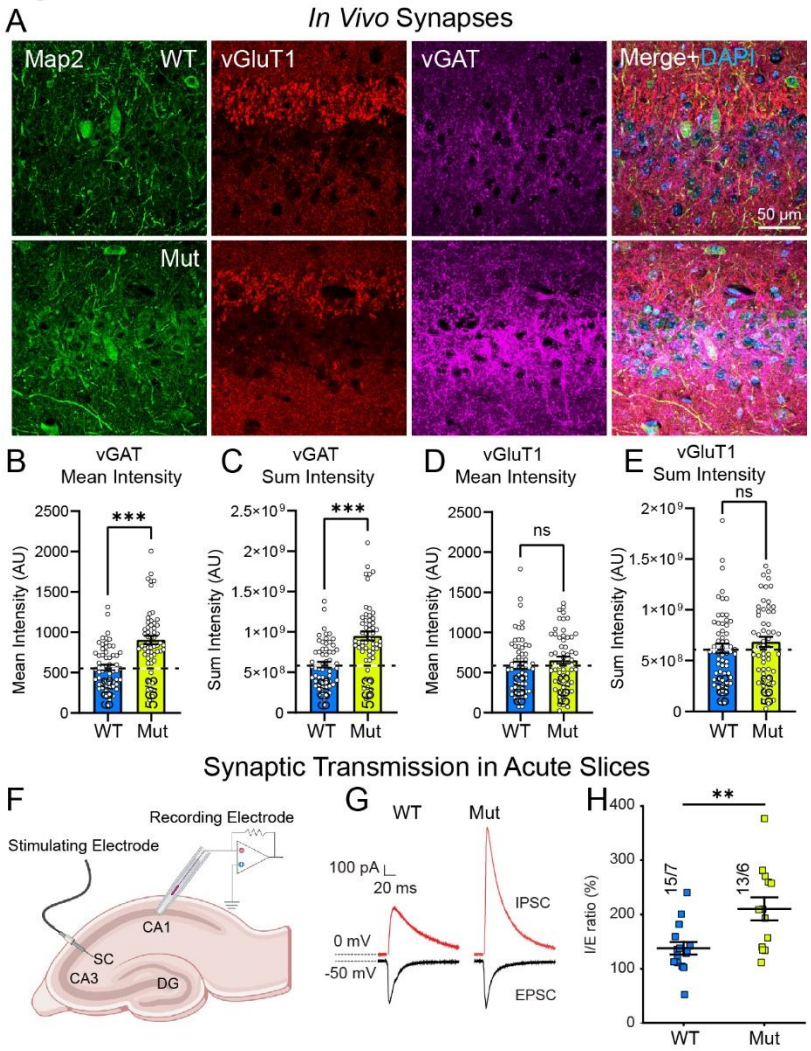

Figure 5: Increased number of functional inhibitory synapses in vivo.

A, Representative micrographs of hippocampal sections showing the CA3 region of WT and Mut mice. Sections are stained for Map2 (green), vGluT1 (red), vGAT (magenta), and Dapi (blue).

B-E, Summary graphs for vGAT and vGluT1 staining showing mean instensity (intensity of all pixels/number of pixels) and the sum intensity of all pixels with the field of view.

F, Experimental paradigm for recordings from acute hippocampal slices of WT and Mut mice.

G and H, Representative traces of evoked IPSC (I) and EPSC (E) amplitudes and the summary graph showing their ratios. WT: 15 cells from 7 mice; Mut: 13 cells from 6 mice were recorded.

Data are individual values (one image in B-E; and one cell in H) and means ± SEM; statistical significance was assessed by two-tailed unpaired Student's t-test (**, $p<0.01$; *** $p<0.001$).

Fig.6

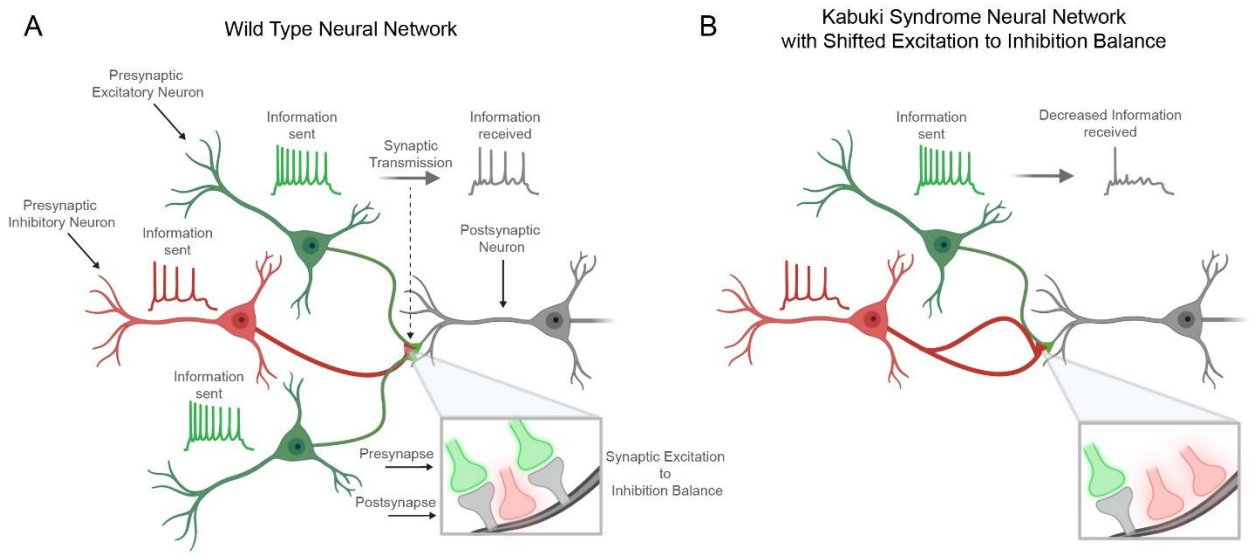

Figure 6: Neural networks in Kabuki syndrome show enhanced inhibitory synaptic development

A, Example network consisting of excitatory (green) and inhibitory neurons (red), promoting and repressing information transfer at synapses (spike diagrams, left vs. right, respectively).

B, Synaptic dysfunction: Due to an overabundance of inhibitory synapses, information transfer through the network is impaired.

SUPPLEMENTARY FIGURES AND FIGURE LEGENDS

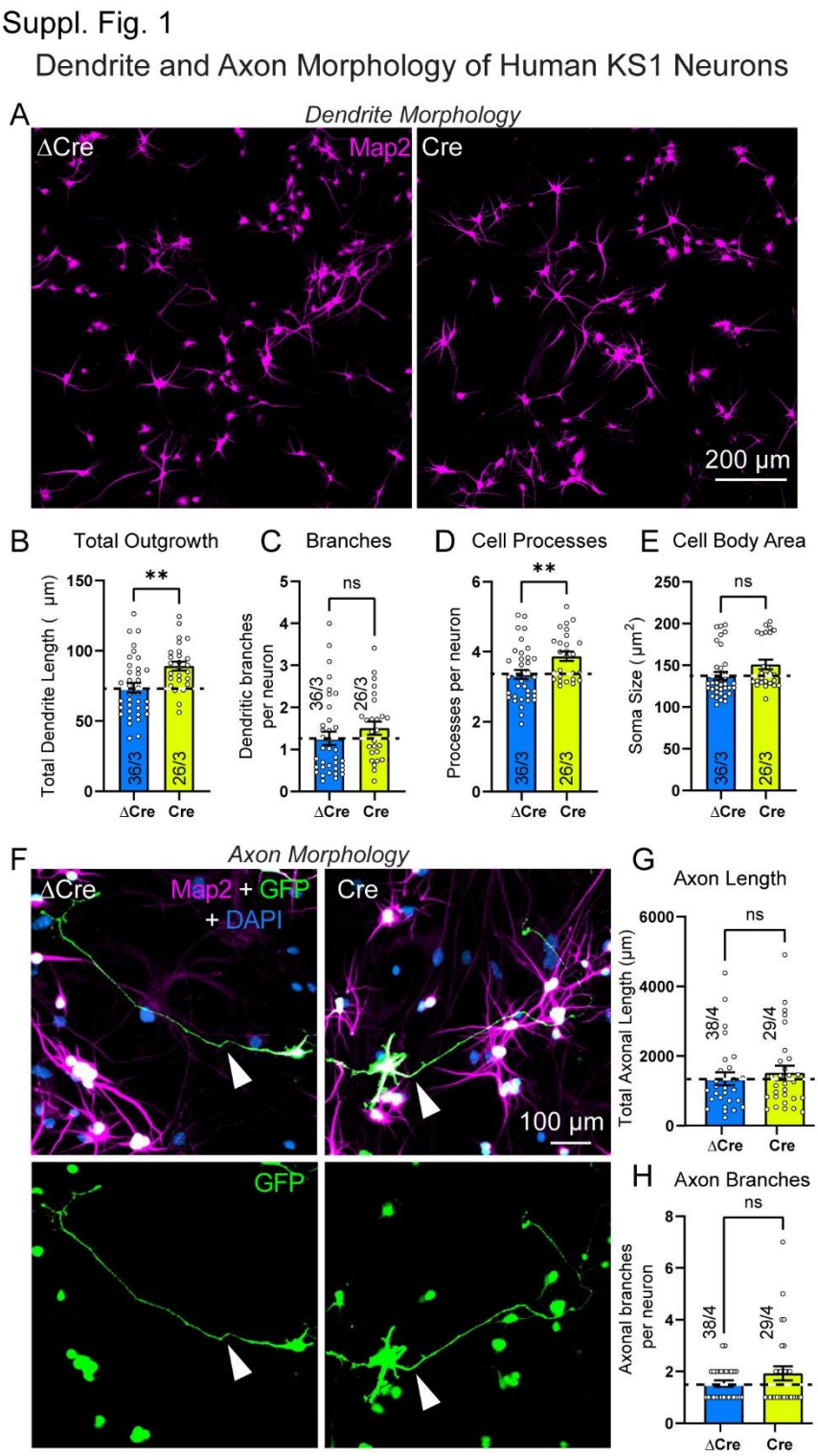

Suppl. Figure 1: Dendrite length and complexity are enhanced in KMT2D-mutant human neurons while no differences were found for axon morphology.

A, Representative images of dendritic morphology in human excitatory neurons stained with MAP2 (magenta) from ΔCre (*KMT2D* wild-type) and Cre (*KMT2D* mutant) cultures at 21 days.

B-E) Quantification of dendritic outgrowth, processes, branches, and soma size in ΔCre and Cre neurons. B, Total dendrite length shows a significant increase in Cre mutant neurons compared to ΔCre neurons (**=p<0.01). C, No significant differences in dendritic branches per neuron between ΔCre and Cre neurons. D, Number of cell processes per neuron is significantly increased in Cre mutant neurons (**=p<0.01). E, Cell body area (soma size) also shows no significant differences between ΔCre and Cre neurons.

F, Representative images of axonal morphology in NGN2 neurons at day 21, with dendrites stained by MAP2 (magenta), nuclei stained with DAPI (blue), and axons visualized via sparse EGFP- transfection (green) in ΔCre and Cre neurons (with green nuclei due to ΔCre-GFP and Cre-GFP fusion proteins).

G, No significant differences in total axon length between ΔCre and Cre neurons.

H, No significant differences in the number of axon branches per neuron between ΔCre and Cre neurons.

Data are individual values and means ± SEM; statistical significance was assessed by two-tailed unpaired Student's t-test.

Suppl. Fig.2

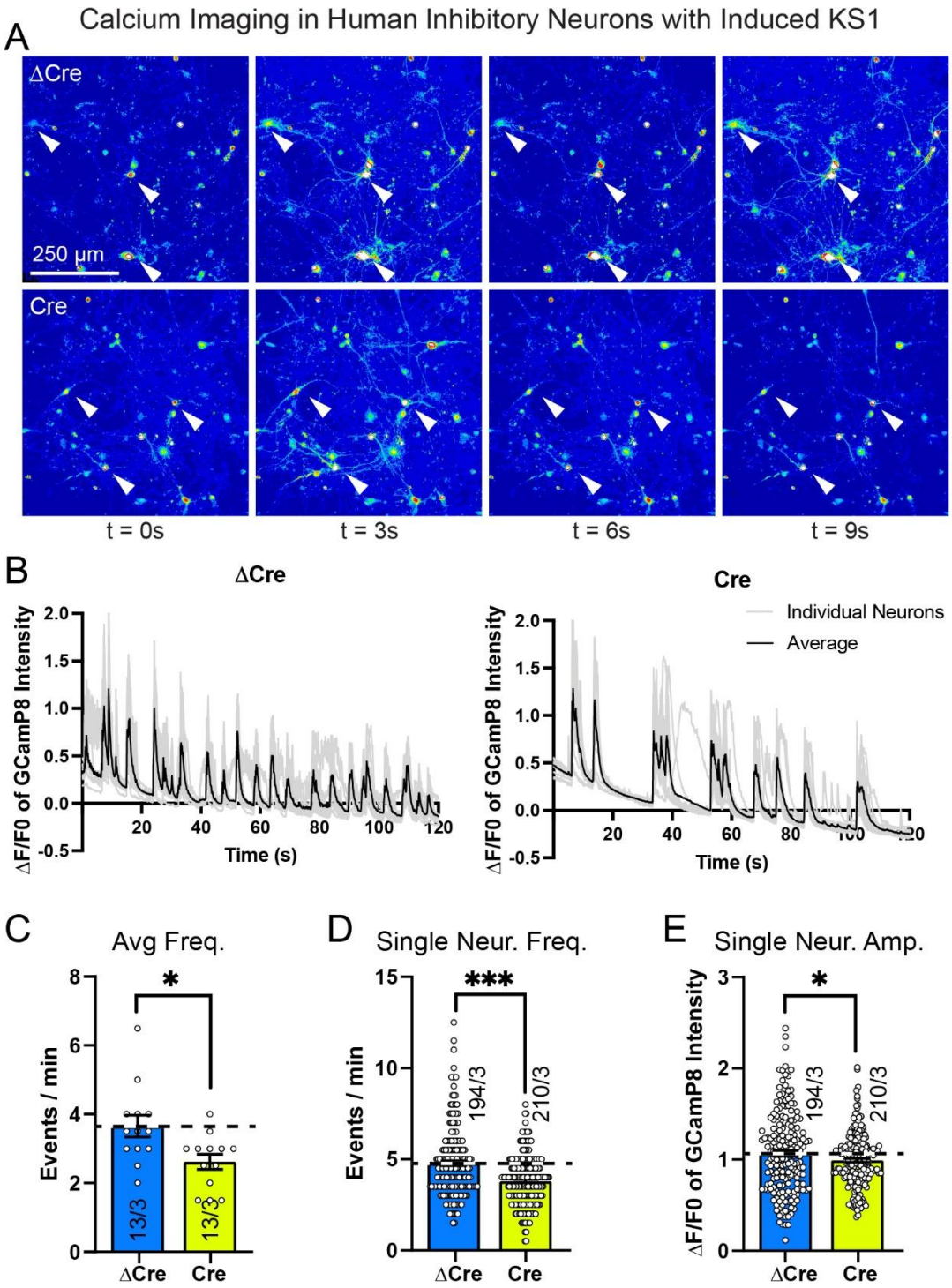

Suppl. Figure 2: Mutation of *KMT2D* leads to overall decreases in calcium activity in human inhibitory neurons.

A, Representative calcium imaging snapshots showing changes in calcium activity in wild-type (ΔCre) and mutant (Cre) inhibitory human induced neurons over time (t = 0, 3, 6, and 9 seconds).

Calcium activity is indicated by changes in gCaMP8m fluorescence intensity, with arrows pointing to regions of active neurons. Neuronal activity was induced by 2.5 mM KCl and 2 mM $CaCl_2$.

B, Calcium event traces of gCaMP8m intensity ($\Delta F/F_0$) over 120 seconds in ΔCre and Cre neurons. Each spike represents a calcium event, with Cre neurons showing decreased frequency and heightened amplitude compared to ΔCre neurons.

C-E, Quantification of calcium event frequency and amplitude in ΔCre and Cre neurons. C, Average frequency (events/min), representing calcium activity across multiple neurons, shows a significant decrease in Cre neurons compared to ΔCre neurons (*=$p<0.05$). D, Single neuron frequency shows a significant decrease in Cre neurons compared to ΔCre neurons (***=$p<0.001$). E, Single neuron amplitude ($\Delta F/F_0$ of GCaMP8m intensity) shows a significant decrease in Cre neurons compared to ΔCre neurons.

Data are individual values and means ± SEM; statistical significance was assessed by two-tailed unpaired Student's t-test.

Suppl. Fig. 3

Dendrite and Axon Morphology of Human KS2 Neurons

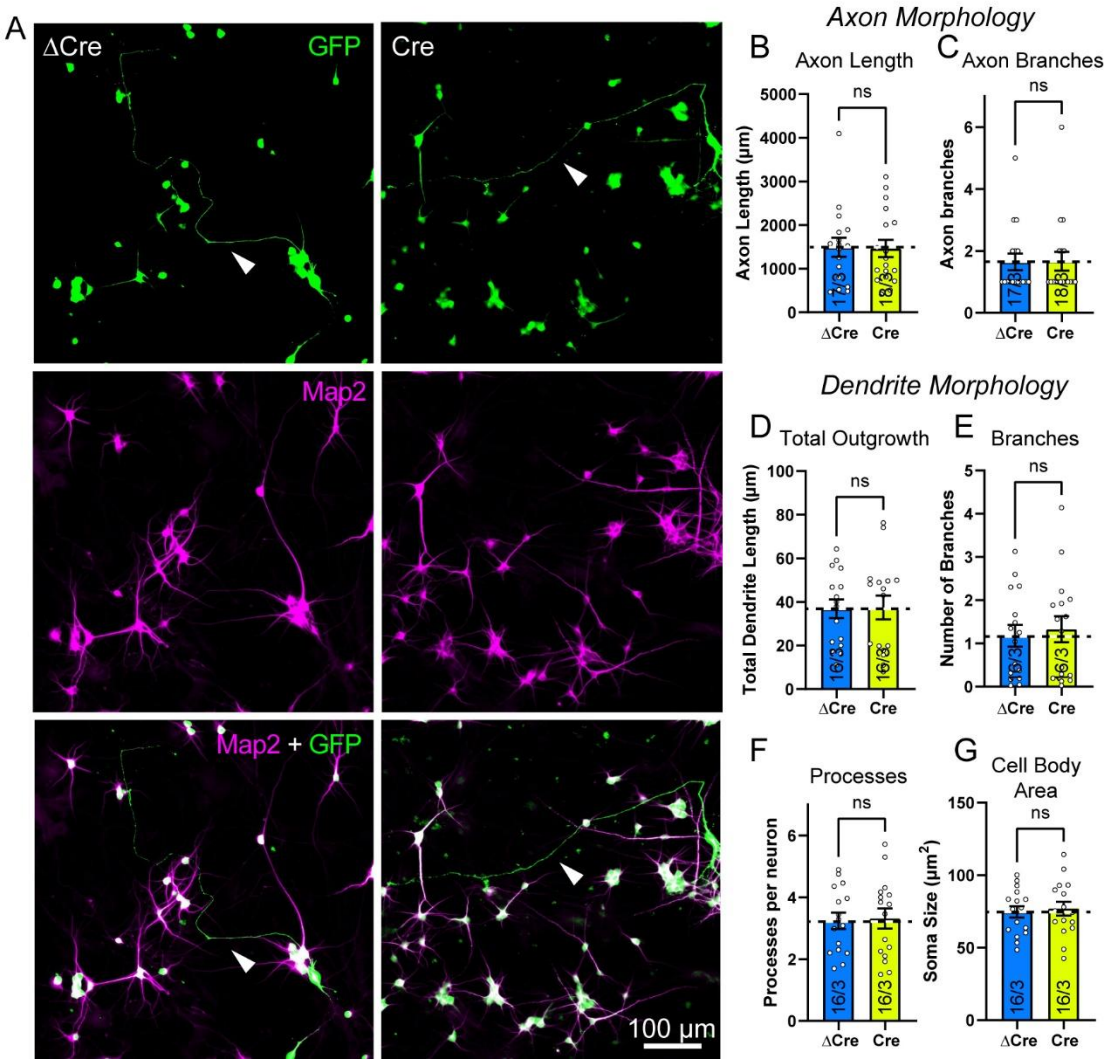

Suppl. Figure 3: Conditional mutation of UTX in human excitatory neurons leads to no differences in dendrite or axon morphology.

A, Representative images of axon and dendrite morphology in ΔCre (UTX wild-type) and Cre (UTX mutant) Ngn2-derived neurons at DIV21. Composite images (bottom row) display sparse overexpression of EGFP (green, marking axons) and MAP2 (magenta, marking dendrites), with arrows indicating axonal structures. EGFP images (middle row) show axonal structures (green), while MAP2 images (bottom row) depict dendritic structures (magenta) in ΔCre and Cre neurons.

B-G, Quantification of axonal and dendritic properties in ΔCre and Cre neurons.

Data are individual values and means ± SEM; statistical significance was assessed by two-tailed unpaired Student's t-test.

Suppl. Fig.4

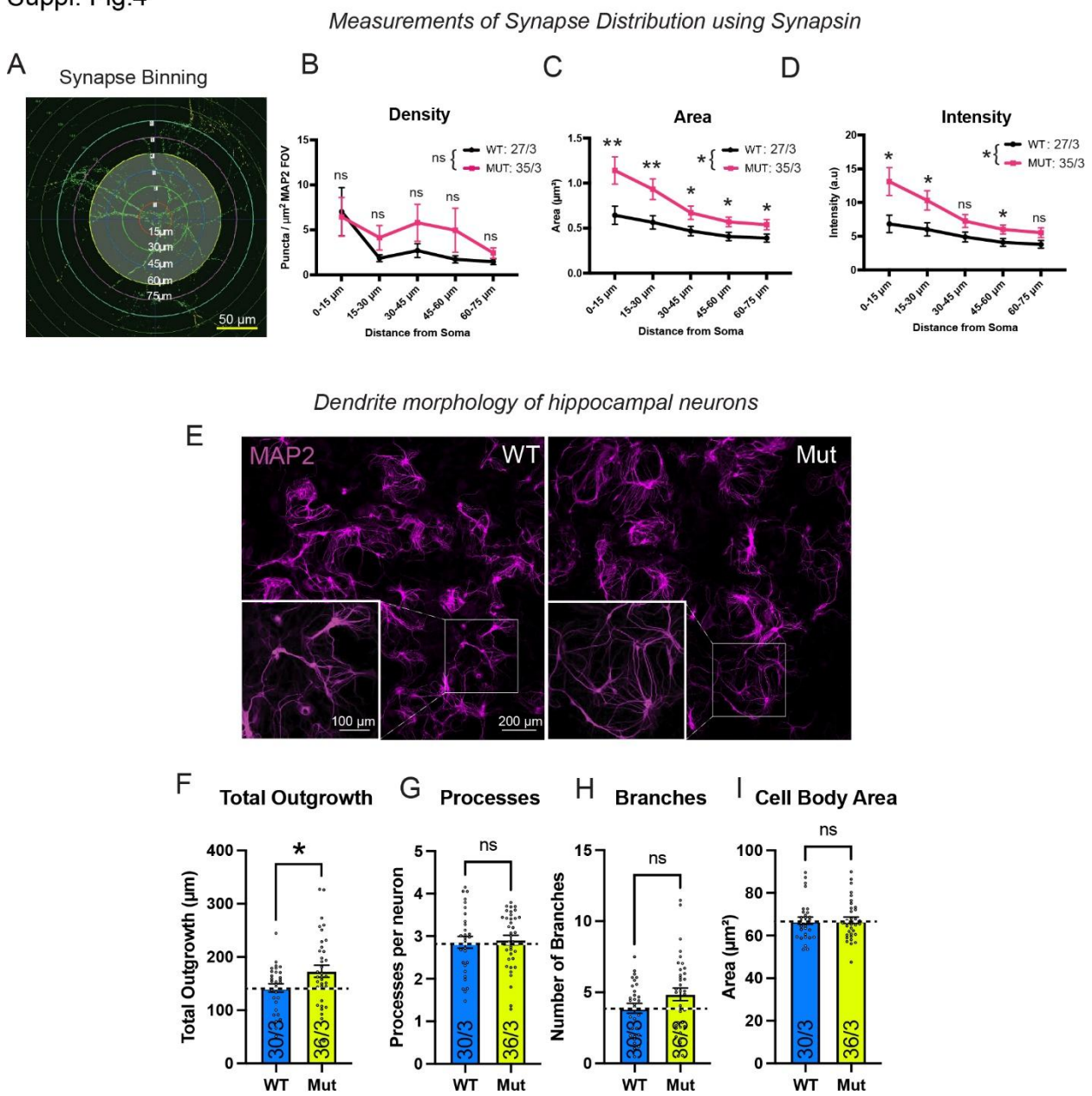

Suppl. Figure 4: Kmt2d mutation leads to changes in overall synapse distribution and increased dendritic arbor in cultured hippocampal neurons.

A, Schematic representation of synapse binning used to measure synapse distribution at different distances from the soma in mouse hippocampal neurons.

B-D, Summary graphs of synaptic puncta density, area, and intensity as a function of distance from the cell soma. Mutant neurons show a greater increase in Synapsin-1 puncta metrics, particularly at distances closest to the soma.

E, Dendritic outgrowth is enhanced in Kmt2d-mutant neurons. Immunocytochemistry images show Map2-labeled dendrites in wild-type (WT) and mutant (Mut) hippocampal neurons cultured

for 2 weeks. The left panel shows WT neurons, and the right panel shows Mut neurons. Insets provide zoomed-in views of dendritic structures.

F-I, Quantification of dendritic morphology in WT and Mut neurons: F, Mutant neurons show a significant increase in total dendritic outgrowth compared to WT neurons. G, No significant difference in the number of processes per neuron (ns = not significant). H, There was no significant difference in dendritic branching between WT and Mut neurons. I, No significant difference was observed in the cell body area between WT and Mut neurons.

Data are presented as individual values and/or means ± SEM; statistical significance in B-D and F-I was assessed by two-tailed unpaired Student's t-test (*, $p<0.05$; **, $p<0.01$) and additionally in B-D by two-way ANOVA repeated-measurements (*, $p<0.05$).

Suppl. Fig.5

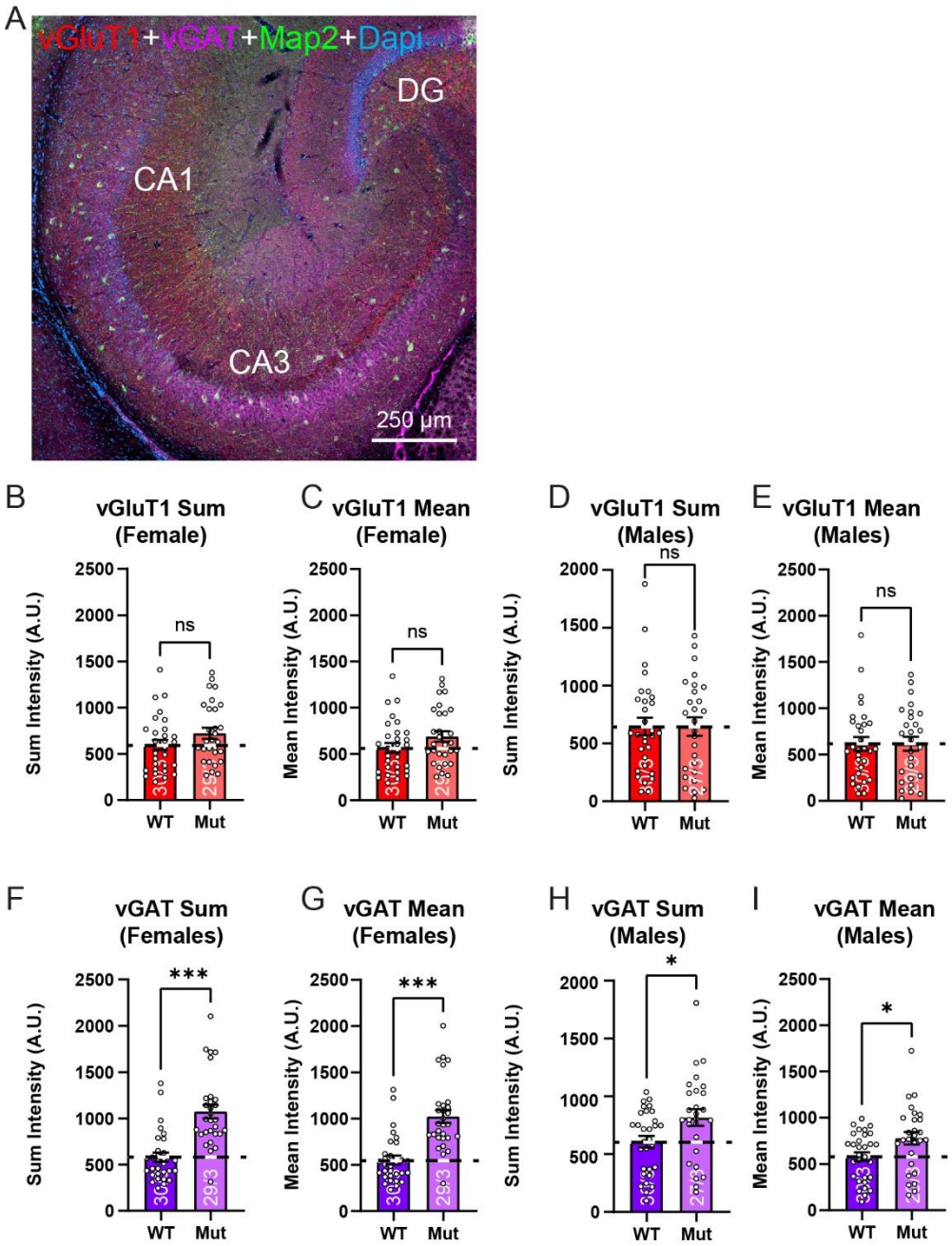

Suppl. Figure 5: Increased number of inhibitory synapses in male and female mice *in vivo*.

A, Overview image of hippocampal formation in a young adult (P30) WT mouse. Section were stained for Map2 (green), vGluT1 (red), vGAT (magenta), and Dapi (blue).

B-I, Summary graphs for vGAT and vGluT1 staining showing mean instensity (intensity of all pixels/number of pixels) and the sum intensity of all pixels with the field of view. Images analyzed correspond to those shown in Figure 3A. Data here are identical to Figure 3B-E but are separated into male and female mice.

Data are presented as individual values (one image) and means ± SEM; statistical significance was assessed by two-tailed unpaired Student's t-test (*, $p<0.05$; *** $p<0.001$).